

Mirror-Descent Inverse Kinematics for Box-constrained Joint Space

Taisuke Kobayashi¹

Abstract—This paper proposes a new Jacobian-based inverse kinematics (IK) explicitly considering box-constrained joint space. To control humanoid robots, the reference pose of end effector(s) is planned in task space, then mapped into the reference joints by IK. Due to the limited analytical solutions for IK, iterative numerical IK solvers based on Jacobian between task and joint spaces have become popular. However, the conventional Jacobian-based IK does not explicitly consider the joint constraints, and therefore, they usually clamp the obtained joints during iteration according to the constraints in practice. The problem in clamping operation has been pointed out that it causes numerical instability due to non-smoothed objective function. To alleviate the clamping problem, this study explicitly considers the joint constraints, especially the box constraints in this paper, inside the new IK solver. Specifically, instead of clamping, a mirror descent (MD) method with box-constrained real joint space and no-constrained mirror space is integrated with the conventional Jacobian-based IK methods, so-called MD-IK. In addition, to escape local optima nearby on the boundaries of constraints, a heuristic technique, called ϵ -clamping, is implemented as margin in software level. As a result, MD-IK achieved more stable and enough fast i) regulation on the random reference poses and ii) tracking to the random trajectories compared to the conventional IK solvers.

I. INTRODUCTION

With increasing performance of robots and decreasing the number of workers, various robots and methods have been developed to replace various human tasks by robots. In particular, humanoid robots have long been studied because they can be introduced without changing human-living environments and are expected to be highly versatile [1], [2]. To accomplish a given task by a humanoid robot, the major approach is to plan and generate the intuitive reference poses in task space (i.e. Cartesian space for the end effector(s) of the robot), not to directly control the robot in joint space. In this major approach, for example, the robot can easily plan the reference poses to avoid obstacles [3], [4].

From the reference poses, the reference joints are computed basically through inverse kinematics (IK) [5], [6]. Only in limited cases, closed-form solutions of IK can be obtained. Especially in humanoid robots, however, the joints activated in IK is task-dependent, so it is infeasible to prepare all the closed-form solutions for all the combinations of the activated joints in advance. Therefore, iterative numerical IK solvers [7]–[11] are more popular for general use. In particular, the IK solvers with Jacobian between the task and joint spaces (e.g. [7]) are practically useful in terms of convergence speed. Such Jacobian-based IK has frequently been employed in humanoid robot control [12], [13].

However, when using Jacobian-based IK, we have to take care of its practical implementation. Since it is a kind of gradient descent method, the computed reference joints would be in the whole real space, not in the joint space. The joint space generally has constraints, i.e. upper and lower limits for each joint and maximum (angular) velocity for each, hence the constraints should be taken into account every iteration of Jacobian-based IK. In practice, such constraints are satisfied with clamping the reference joints. The numerical instability has been, however, reported due to non-smoothed objective function by clamping operation [8].

To alleviate this clamping problem, TRAC-IK [8] proposes the use of nonlinear optimizer, which is robust to non-smooth objective function. TRAC-IK has been established as one of the popular IK solvers, but it still remain the clamping problem. In addition, from the viewpoint of calculation cost, the nonlinear optimization is combined with the conventional Jacobian-based IK, thereby making tuning complicated.

In contrast, Drexler and Harmati [9] introduces additional non-constrained variables, which are nonlinearly mapped from the box-constrained joint space and are optimized by Jacobian-based updates. After optimization of that variables, the reference joints can be obtained by inversely mapping it without any clamping. However, this approach has slow convergence due to the gradients added by nonlinear mapping.

In machine learning fields, the clamping operation and the above mapping technique can be regarded as a gradient projection method [14] and a parameterization method, which is frequently used in neural networks, respectively. By organizing the conventional methods from this perspective, a new method, i.e. mirror descent (MD) method [15], [16], can naturally emerge. MD is a kind of generalized version of gradient descent for Bregman divergence minimization. In practice, it can handle the constrained space as like the parameterization method [9], while maintaining the similar convergence speed to the gradient projection method [8].

This paper therefore proposes the algorithm to integrate the conventional Jacobian-based IK with MD for joint constraints (box constraints as the first step of this study), so-called MD-IK (see Fig. 1). MD-IK is implemented with two design-related contributions as follows:

- 1) Nonlinear mapping between the non-constrained mirror space and the box-constrained joint space is designed with mathematical derivation.
- 2) A heuristic technique, called ϵ -clamping, is introduced in order to escape from local optima caused nearby on the boundaries of constraints.

Here, the second corresponds to the software-level margin.

¹Taisuke Kobayashi is with the Division of Information Science, Nara Institute of Science and Technology, 8916-5 Takayama-cho, Ikoma, Nara 630-0192, Japan kobayashi@is.naist.jp

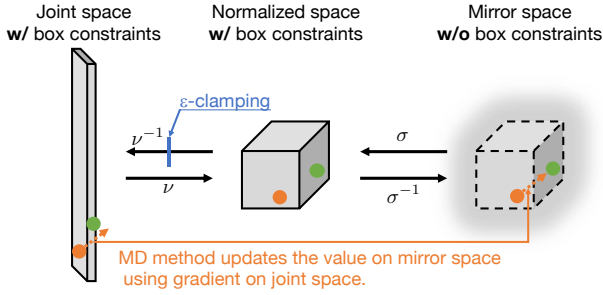


Fig. 1. Conceptual scheme of MD-IK: the reference on the constrained joint space is transformed into the unconstrained mirror space via the normalized space; the transformed reference is updated using the gradients on the joint space; the updated reference is inversely transformed into the joint space; in that time, ϵ -clamping is heuristically applied to escape from the local solutions near the boundaries.

For verification of MD-IK implemented on Pinocchio library [17], i) regulation and ii) tracking tasks are conducted with different types of robots [18]–[20]. In comparison with the gradient projection (a.k.a. the clamping method) and the parameterization method, we can see that MD-IK achieves more stable and enough fast i) regulation on the random reference poses and ii) tracking to the random trajectories. In addition, thanks to that ability, only MD-IK can achieve good success rate for convergence even with Jacobian-transpose (JT) IK [5], which is known as easier but slower method than Levenberg-Marquardt (LM) IK [7].

II. PRELIMINARIES

A. Jacobian-based inverse kinematics

Here, the conventional Jacobian-based IK [5], [6] is briefly introduced. The end effector pose as the combination of position $\mathbf{p}(\mathbf{q}) \in \mathbb{R}^3$ and orientation $Q(\mathbf{q})$ (unit quaternion) can be given as the functions of joint configurations $\mathbf{q} = [q_1, \dots, q_i, \dots, q_N]^\top$ with N active joints. Given the reference pose as \mathbf{p}^{ref} and Q^{ref} , the errors $\mathbf{e} \in \mathbb{R}^6$ between it and the current pose is also regarded as the function of \mathbf{q} as follows:

$$\mathbf{e}(\mathbf{q}) = \begin{bmatrix} \mathbf{p}^{\text{ref}} - \mathbf{p}(\mathbf{q}) \\ f(Q^{\text{ref}} * Q^{-1}(\mathbf{q})) \end{bmatrix} \quad (1)$$

where $f(\cdot) \in \mathbb{R}^3$ denotes the rotation vector representation. The objective of IK is to find \mathbf{q}^* via the following minimization problem.

$$\mathbf{q}^* = \arg \min_{\mathbf{q}} E(\mathbf{q}) \quad (2)$$

$$E(\mathbf{q}) = \frac{1}{2} \mathbf{e}(\mathbf{q})^\top W \mathbf{e}(\mathbf{q})$$

where W denotes the diagonal weight matrix.

To minimize this problem, the gradient descent method is one choice. Specifically, the gradients $\mathbf{g}(\mathbf{q}) = \partial E / \partial \mathbf{q} \in \mathbb{R}^N$ can be approximated as follows:

$$\mathbf{g}(\mathbf{q}) = -J^\top(\mathbf{q}) W \mathbf{e}(\mathbf{q}) \quad (3)$$

where $J \in \mathbb{R}^{6 \times N}$ denotes Jacobian between the pose and the corresponding joint configurations. Using \mathbf{g} , the reference

joint configurations \mathbf{q}^{ref} are iteratively updated with the step size $\alpha > 0$.

$$\mathbf{q}^{\text{ref}} \leftarrow \mathbf{q}^{\text{ref}} - \alpha \mathbf{g}(\mathbf{q}^{\text{ref}}) \quad (4)$$

where the initial \mathbf{q}^{ref} should be given as like the observed joint configurations \mathbf{q}^{obs} . Until convergence (i.e. $E < \delta$ with δ threshold) or time limit, the above update is iterated. This method is the Jacobian transpose (JT) method since the gradients in the method are computed with J^\top .

Actually, the JT method has poor convergence performance, such as too slow convergence speed and/or oscillated behavior. For further improvement, the Newton-Raphson method with the Hessian matrix $H \in \mathbb{R}^{N \times N}$ inversely multiplied with the gradients are often employed. H^{-1} is, however, numerically unstable in the vicinity of the singular postures. The manipulated Hessian matrix \tilde{H} is therefore designed based on Levenberg-Marquardt (LM) method for stable computation [7].

$$\tilde{H}(\mathbf{q}) = J^\top(\mathbf{q}) W J(\mathbf{q}) + D(\mathbf{q}) \quad (5)$$

$$D(\mathbf{q}) = (\lambda + E(\mathbf{q})) I \quad (6)$$

where the diagonal $D \in \mathbb{R}^{N \times N}$ denotes the damping factor with $\lambda > 0$ the minimum damping factor for numerical stability. \tilde{H} is now always invertible, and if the minimization target E is larger mainly in the vicinity of the singular points, \tilde{H}^{-1} will be smaller and reduce the update amount. Using \tilde{H} , the gradients to be used for updating \mathbf{q}^{ref} are redefined from eq. (3) as follows:

$$\mathbf{g}(\mathbf{q}) = -\tilde{H}^{-1}(\mathbf{q}) J^\top(\mathbf{q}) W \mathbf{e}(\mathbf{q}) \quad (7)$$

As well as the JT method, this method (called the LM method in this paper) iteratively updates \mathbf{q}^{ref} until convergence or time limit.

B. Clamping for box-constrained joint space

In practice, the joint configurations \mathbf{q} are constrained mainly by upper and lower limits, \mathbf{q}^{low} and \mathbf{q}^{up} respectively, and maximum (angular) velocities $\dot{\mathbf{q}}^{\text{max}}$. This paper, therefore, considers the following box constraints.

$$\underline{\mathbf{q}} \leq \mathbf{q} \leq \bar{\mathbf{q}} \quad (8)$$

where

$$\underline{\mathbf{q}} = \max(\mathbf{q}^{\text{low}}, \mathbf{q}^{\text{obs}} - \dot{\mathbf{q}}^{\text{max}} dt) \quad (9)$$

$$\bar{\mathbf{q}} = \min(\mathbf{q}^{\text{up}}, \mathbf{q}^{\text{obs}} + \dot{\mathbf{q}}^{\text{max}} dt) \quad (10)$$

where dt denotes the time step for control.

When \mathbf{q}^{ref} is updated by eq. (4) with eq. (3) or (7), it may violate this constraints since the gradients are in real space and the update law just subtracts them from \mathbf{q}^{ref} . In practical implementations to satisfy the constraints, the following clamping operation is conducted for \mathbf{q}^{ref} after each update iteration with eq. (3) or (7).

$$\mathbf{q}^{\text{ref}} \leftarrow \max(\min(\mathbf{q}^{\text{ref}}, \bar{\mathbf{q}}), \underline{\mathbf{q}}) \quad (11)$$

Note that the overview of the above conventional IK solvers is summarized in Alg. 1.

Algorithm 1 Conventional Jacobian-based IK

- 1: Get the constraints \mathbf{q}^{low} , \mathbf{q}^{up} , and $\dot{\mathbf{q}}^{\text{max}}$ from model
 - 2: Set hyperparameters W , α , λ , δ , and dt
 - 3: Set the reference pose \mathbf{p}^{ref} and Q^{ref}
 - 4: Observe the joint configurations \mathbf{q}^{obs}
 - 5: Set the lower bound $\underline{\mathbf{q}}$ by eq. (9)
 - 6: Set the upper bound $\bar{\mathbf{q}}$ by eq. (10)
 - 7: $\mathbf{q}^{\text{ref}} = \mathbf{q}^{\text{obs}}$
 - 8: Set t_s as the current time t
 - 9: **while** True **do**
 - 10: Compute the errors $\mathbf{e}(\mathbf{q}^{\text{ref}})$ by eq. (1)
 - 11: Compute the minimization target $E(\mathbf{q}^{\text{ref}})$ by eq. (2)
 - 12: **if** ($E(\mathbf{q}^{\text{ref}}) < \delta$) or ($t - t_s > dt$) **then break**
 - 13: Compute Jacobian $J(\mathbf{q}^{\text{ref}})$ using model
 - 14: Compute the gradients $\mathbf{g}(\mathbf{q}^{\text{ref}})$ by eq. (3) or (7)
 - 15: Update \mathbf{q}^{ref} by eq. (4)
 - 16: Clamp \mathbf{q}^{ref} by eq. (11)
 - 17: **end while**
 - 18: **Return** \mathbf{q}^{ref}
-

C. Mirror descent method

The non-smooth minimization problem by the clamping operation would cause several local minima, which would make IK numerically unstable [8]. This paper therefore considers the box constraints in eq. (8) explicitly. To this end, by focusing on the fact that the above Jacobian-based IK is regarded as the (projected) gradient descent method, the MD method [15], [16] is employed. Its brief introduction is described below.

The MD method supposes the existence of mirror space, where the variables \mathbf{q} in main space (i.e. joint space in IK) can be mapped through nonlinear invertible mapping function as the mirror variables $\boldsymbol{\rho} = \psi(\mathbf{q})$ with the same dimension size as \mathbf{q} . Although this mapping function is theoretically derived as the derivative of some Bregman divergences D_ψ , we can use the MD method with the arbitrary invertible function. Given the minimization target $E(\mathbf{q})$, the update law of \mathbf{q} is summarized as follows:

$$\boldsymbol{\rho} \leftarrow \boldsymbol{\rho} - \alpha \frac{\partial E(\mathbf{q})}{\partial \mathbf{q}}, \quad \mathbf{q} \leftarrow \psi^{-1}(\boldsymbol{\rho}) \quad (12)$$

Alternatively, the case without explicitly defining $\boldsymbol{\rho}$ is equivalently given.

$$\mathbf{q} \leftarrow \psi^{-1} \left(\psi(\mathbf{q}) - \alpha \frac{\partial E(\mathbf{q})}{\partial \mathbf{q}} \right) \quad (13)$$

As a remark, if $\partial E(\psi^{-1}(\boldsymbol{\rho}))/\partial \boldsymbol{\rho}$ is utilized instead of $\partial E(\mathbf{q})/\partial \mathbf{q}$, that method is consistent with the parameterization method. That is, $\boldsymbol{\rho}$ is updated by the standard gradient descent method, and then, the updated value is mapped to \mathbf{q} as the new value. Indeed, the previous work [9] derives the gradients of $\boldsymbol{\rho}$ by multiplying Jacobian over \mathbf{q} with $\partial \psi^{-1}(\boldsymbol{\rho})/\boldsymbol{\rho}$. It is noticed that this multiplied gradient $\partial \psi^{-1}(\boldsymbol{\rho})/\boldsymbol{\rho}$ is expected to be less than 1 for the mapping function suitable for the box constraints like in this study. Hence, the previous work has poor convergence speed.

III. PROPOSAL: MD-IK

A. Mapping between real joint and mirror spaces

The proposed method, MD-IK, integrates the MD method with the Jacobian-based IK in order to explicitly consider the box-constrained joint space. For this integration, the invertible mapping function ψ should be designed so that ψ^{-1} maps real value on the mirror real space to one on the box-constrained joint space within $[\underline{\mathbf{q}}, \bar{\mathbf{q}}]$.

Such nonlinear mapping functions can be designed by using element-wise sigmoid function σ , such as logistic function and error function. In general, however, the sigmoid function is a map to $[0, 1]$ (or $[-1, 1]$), and therefore, the denormalization function ν^{-1} is also required. That is, the mapping function ψ can be given as the following composite function of the inverted sigmoid function and the normalization function.

$$\psi = \sigma^{-1} \circ \nu \quad (14)$$

$$\nu(\mathbf{q}) = \frac{\mathbf{q} - \underline{\mathbf{q}}}{\bar{\mathbf{q}} - \underline{\mathbf{q}}} \quad (15)$$

From the definition of ν , we can easily compute ν^{-1} as the denormalization function, $\mathbf{q} = (\bar{\mathbf{q}} - \underline{\mathbf{q}})\nu(\mathbf{q}) + \underline{\mathbf{q}}$. Using the above functions, the general update law of MD-IK is derived as follows:

$$\begin{aligned} \mathbf{q}^{\text{ref}} &\leftarrow \psi^{-1} \left(\psi(\mathbf{q}^{\text{ref}}) - \alpha \mathbf{g}(\mathbf{q}^{\text{ref}}) \right) \\ &= (\bar{\mathbf{q}} - \underline{\mathbf{q}}) \sigma \left(\sigma^{-1} \left(\frac{\mathbf{q}^{\text{ref}} - \underline{\mathbf{q}}}{\bar{\mathbf{q}} - \underline{\mathbf{q}}} \right) - \alpha \mathbf{g}(\mathbf{q}^{\text{ref}}) \right) + \underline{\mathbf{q}} \end{aligned} \quad (16)$$

Although one example of σ is introduced later, its heuristic conditions are given as below. Specifically, since only the normalized value (minus the gradient) is fed into σ , it is desired for σ to output roughly $(0, 1)$ in that range to fully use the entire range of σ . This requirement leads to the following conditions with a threshold $\epsilon \ll 1$.

$$\sigma(0) = \epsilon, \quad \sigma(1) = 1 - \epsilon \quad (17)$$

σ designed under the above conditions and its inverse σ^{-1} are illustrated in Fig. 2. As can be seen, almost the entire function shapes are contained within $[0, 1]$.

B. Special case with logistic function

As an example of the sigmoid function, the following logistic function, which is well known as the representative in both robotics and machine learning fields, is considered.

$$\sigma(x) = \frac{1}{1 + \exp(-a(x - b))} \quad (18)$$

where a and b are the parameters designed according to eq. (17) as follows:

$$a = 2 \log \frac{1 - \epsilon}{\epsilon}, \quad b = \frac{1}{2} \quad (19)$$

The inverse function of this logistic function, called logit function, is given by the following formula.

$$\sigma^{-1}(x) = -\frac{1}{a} \log \frac{1 - x}{x} + b \quad (20)$$

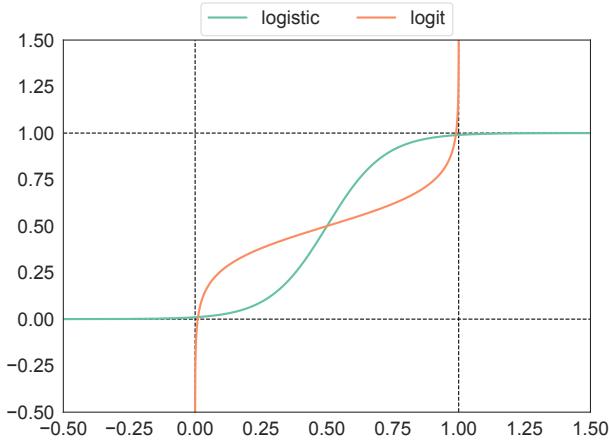


Fig. 2. Example of sigmoid function σ and its inverse σ^{-1} : the logistic and logit functions shown in eqs. (18)–(20) are visualized; their domains can easily be understandable, $\sigma : \mathbb{R} \rightarrow [0, 1]$ and $\sigma^{-1} : [0, 1] \rightarrow \mathbb{R}$; by eq. (17), both functions are given almost the entire structure in $[0, 1]$.

Using these functions, eq. (16) can be solved more specifically. That is, the update law of MD-IK with the logistic function described in eqs. (18)–(20) is derived (details are in Appendix A).

$$\mathbf{q}^{\text{ref}} \leftarrow (\bar{\mathbf{q}} - \underline{\mathbf{q}}) \frac{\mathbf{q}^{\text{nom}}}{\mathbf{q}^{\text{nom}} + (1 - \mathbf{q}^{\text{nom}}) \exp(a\alpha \mathbf{g}(\mathbf{q}^{\text{ref}}))} + \underline{\mathbf{q}} \quad (21)$$

where $\mathbf{q}^{\text{nom}} = \nu(\mathbf{q}^{\text{ref}}) = (\mathbf{q}^{\text{ref}} - \underline{\mathbf{q}})/(\bar{\mathbf{q}} - \underline{\mathbf{q}})$ for simplicity. As can be seen from the above equation, only a in the design parameters of the logistic function is involved in the update as the additional step size.

C. ϵ -clamping as margin in software level

The MD method with the above sigmoid function yields the smooth update without clamping. On the other hand, it makes the update difficult to escape nearly on the boundaries. Indeed, as can be seen in eq. (21), if $\mathbf{q}^{\text{nom}} \simeq 1$ (i.e. $\mathbf{q}^{\text{ref}} \simeq \bar{\mathbf{q}}$), the effect of the gradients will be almost disappeared; and if $\mathbf{q}^{\text{nom}} \simeq 0$ (i.e. $\mathbf{q}^{\text{ref}} \simeq \underline{\mathbf{q}}$), the fractional term including the gradients term will be almost zero. To mitigate this local optima problem, a heuristic technique, called ϵ -clamping, is implemented.

Specifically, the following clamping with ϵ is applied after each update.

$$\mathbf{q}^{\text{ref}} \leftarrow \nu^{-1}(\max(\min(\nu(\mathbf{q}^{\text{ref}}), 1 - \epsilon), \epsilon)) \quad (22)$$

This clamping can be regarded as a margin at the software level to avoid boundary values that are not desirable for commands in terms of practical joint control performance. For example, the maximum velocity is a catalog specification and would not be performed, and the hardware boundaries would cause mechanical collisions. In addition, in terms of smoothness, the effect of this clamping is insignificant since the gradients on the clamped range converges to almost zero when σ is designed according to eq. (17).

Algorithm 2 MD-IK: the differences from Alg. 1 are with underline.

- 1: Get the constraints \mathbf{q}^{low} , \mathbf{q}^{up} , and $\dot{\mathbf{q}}^{\text{max}}$ from model
- 2: Set hyperparameters W , α , λ , δ , and dt
- 3: Set the threshold ϵ
- 4: Set the reference pose \mathbf{p}^{ref} and Q^{ref}
- 5: Observe the joint configurations \mathbf{q}^{obs}
- 6: Set the lower bound $\underline{\mathbf{q}}$ by eq. (9)
- 7: Set the upper bound $\bar{\mathbf{q}}$ by eq. (10)
- 8: $\mathbf{q}^{\text{ref}} = \mathbf{q}^{\text{obs}}$
- 9: Set t_s as the current time t
- 10: **while** True **do**
- 11: Compute the errors $e(\mathbf{q}^{\text{ref}})$ by eq. (1)
- 12: Compute the minimization target $E(\mathbf{q}^{\text{ref}})$ by eq. (2)
- 13: **if** ($E(\mathbf{q}^{\text{ref}}) < \delta$) or ($t - t_s > dt$) **then break**
- 14: Compute Jacobian $J(\mathbf{q}^{\text{ref}})$ using model
- 15: Compute the gradients $\mathbf{g}(\mathbf{q}^{\text{ref}})$ by eq. (3) or (7)
- 16: Update \mathbf{q}^{ref} by eq. (21)
- 17: Clamp \mathbf{q}^{ref} by eq. (22) with ϵ
- 18: **end while**
- 19: Return \mathbf{q}^{ref}

In summary, the pseudo code of MD-IK with the logistic function is described in Alg. 2, while emphasizing the differences from Alg 1 with underline. Comparing with Alg 1, we can see that only the update equations are different. Note that although ϵ has also been added as a new hyperparameter for ϵ -clamping in eq. (22), it should also act on Alg 1 instead of the standard clamping in eq. (11) as the margin at the software level.

IV. EXPERIMENT

A. Conditions

In this section, the performance of MD-IK is verified through two tasks: regulation and tracking tasks. In the regulation task, the reference pose is uniformly randomized, and a robot tries to make its end effector converge on that pose from the same initial pose within 2.5 sec. In the tracking task, the robot firstly moves its end effector to the initial reference pose (i.e. the mean of random pose) within 2.5 sec. Then, each component of the reference pose is moved within the given area by a sinusoidal wave (0.25 Hz at maximum, and uniformly randomly given), and the robot tracks it during 12.5 sec. 2000 trials for the regulation task and 500 trials for the tracking task are performed under each condition with different reference pose or trajectory, and the performance of each condition is statistically evaluated. Note that during trials, only box-constraints on joint space are considered and dynamical constraints and self collisions are ignored for simplicity.

Three different robot models are used for this verification, taking into account the effect of structural differences in the robots. Specifically, TALOS [18] is employed as a full-sized humanoid robot with redundant joints. Its left hand is set as the end effector. As a redundant robot with prismatic

TABLE I
ROBOT CONFIGURATIONS

Robot	#Active joints	Reference pose
		x, y, z m roll, pitch, yaw rad
TALOS	10	$0.6 \pm 0.3, 0.1 \pm 0.3, 1.1 \pm 0.3$
		$0.0 \pm 0.3, -\frac{\pi}{2} \pm 0.3, -\frac{\pi}{2} \pm 0.3$
TIAGo	8	$0.55 \pm 0.25, -0.05 \pm 0.25, 0.75 \pm 0.25$
		$0.0 \pm 0.25, -\frac{\pi}{2} \pm 0.25, -\frac{\pi}{2} \pm 0.25$
UR5	6	$0.6 \pm 0.2, 0.0 \pm 0.2, 0.4 \pm 0.2$
		$0.0 \pm 0.2, -\frac{\pi}{2} \pm 0.2, -\frac{\pi}{2} \pm 0.2$

TABLE II
HYPERPARAMETERS FOR IK

Symbol	Meaning	Value
W	Weight matrix for minimization target	I
α	Step size for update	1
λ	Minimum damping factor	1×10^{-3}
δ	Threshold for convergence	1×10^{-10}
dt	Time step for control	5 ms
ϵ	Threshold for ϵ -clamping	1×10^{-2}

joint, TIAGo [19] is employed. Its torso is lifted up/down by a linear actuator. UR5 [20] is finally employed as a six degree-of-freedom robot, IK of which is actually able to be computed analytically. Their configurations about the number of active joints and the area of the reference pose are summarized in Table I.

As comparisons, the combination of the gradient computation methods (i.e. the JT and LM methods) and the box-constraining methods (i.e. the mirror, parameterized, and projected descent methods) are considered. That is, six methods in total are compared with each other and both of the JT-mirror and LM-mirror descent methods are the proposed method (a.k.a. MD-IK). Note that although TRAC-IK [8] has been proposed for alleviating the clamping problem, it additionally requires nonlinear optimizers and is difficult to be fairly compared with others. Hence, it was omitted from this verification.

All the methods were implemented using the Pinocchio library [17], which contains rigid body algorithms mainly for humanoid robots, on python. In particular, its Jacobian computation and helpers for loading and visualizing model were utilized. The core of IK was actually implemented by NumPy. The hyperparameters for all the methods are given in Table II. Note that all the source codes used were uploaded on GitHub: <https://github.com/kbys-t/mdik>.

B. Regulation task

The success (i.e. convergence) rate of each method in the regulation task is shown in Table III. Note that several trials were completely failed by all the methods due to the unreachable poses randomly given, and therefore, they were excluded in evaluation. As can be seen in the table, the JT-mirror, LM-mirror, and LM-projected method can stably reach the reference pose in time regardless of the structural differences. The JT-projected method always failed due to oscillation caused by high step size. The parameterized

TABLE III
SUCCESS RATES IN THE REGULATION TASK

Method	Robot (#reachable trials)		
	TALOS (1824)	TIAGo (974)	UR5 (1496)
JT-mirror	95.8 ± 20.0	89.7 ± 30.4	96.9 ± 17.5
JT-parameterized	0.05 ± 2.34	0 ± 0	0.20 ± 4.48
JT-projected	0 ± 0	0 ± 0	0 ± 0
LM-mirror	86.6 ± 34.1	95.5 ± 20.8	100 ± 0
LM-parameterized	0 ± 0	5.44 ± 22.7	100 ± 0
LM-projected	95.4 ± 20.8	98.4 ± 12.7	100 ± 0

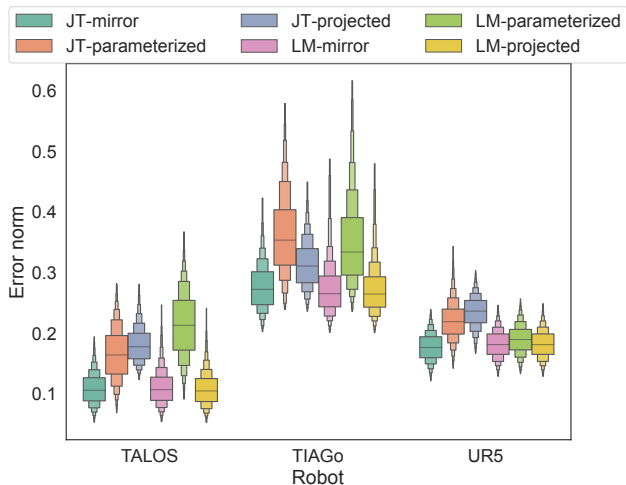


Fig. 3. Error norm in the regulation task: basically, the JT-mirror, LM-mirror, and LM-projected methods performed the comparable results; the worst cases of the JT-mirror method was smaller than the others.

methods basically performed slower convergence than the others. This slowness comes from the additional gradients $\partial q / \partial \rho$ multiplied with the original gradients.

More specifically, the error norm of each method is depicted in Fig. 3. The successful three methods showed almost the comparable errors, however, by focusing on the worse cases, we can see that the JT-mirror method achieved smaller errors than the other two. This result suggests that the JT-mirror method can answer more stable solutions.

Finally, the increase of computational cost is confirmed via Fig. 4, which shows the number of iterations in time (i.e. 5 ms) at first 10 time steps. Since the data is for the time when there is no way to converge, the iterations must be maximized according to the computational cost. Note that all the experiments were conducted with Intel Core i7-9750H. The figure shows that the LM method had higher computational cost due to computation of the inverse of the manipulated Hessian matrix. Among the constraint methods, the difference was not large, and the MD method was in the middle of the other two.

C. Tracking task

The error norm of each method in the tracking task is illustrated in Fig. 5. These were computed with all the trials after initialization. The three methods mentioned above, i.e. the JT-mirror, LM-mirror, and LM-projected methods, also succeeded in making the error enough small. However, in

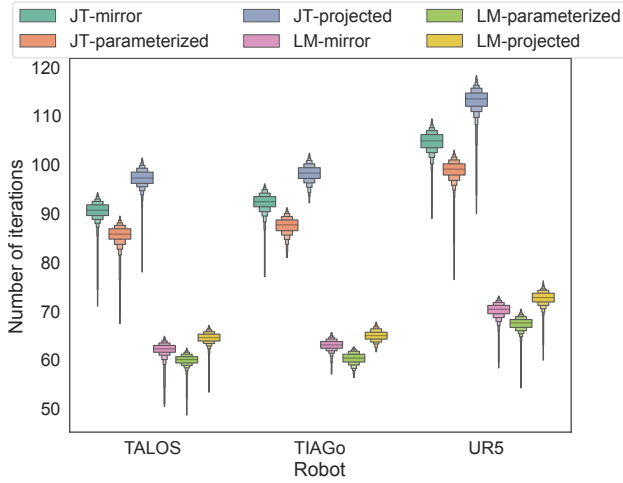


Fig. 4. Number of iteration in the regulation task: the data only at the first 10 time steps were used to show the possible maximum number of iterations; the LM method significantly increased the computational cost from the JT method; compared to that difference, the impact of the constraint method seems to be negligible.

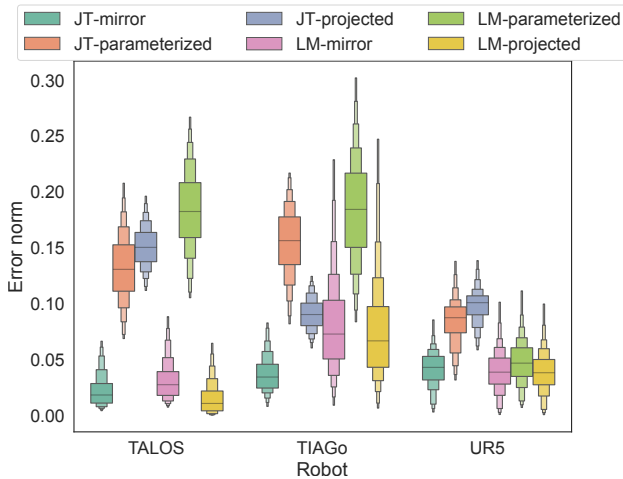


Fig. 5. Error norm in the tracking task: the JT-mirror, LM-mirror, and LM-projected methods made the error enough small; with TIAGo, the JT-mirror method clearly outperformed the others.

the case of TIAGo, where there were many unreachable area compared to the other robots (see Table III), the JT-mirror method clearly obtained the smaller error than the others. This may be because the fact the JT-mirror method kept updating more smoothly even in the vicinity of the singular postures and/or the boundaries of joint constraints.

To confirm the smoothness of trajectories in details, the update amount of the reference joints at each time step is summarized in Fig. 6. Note that the parameterized method achieved the best performance merely due to slow update speed without convergence, and the JT-projected method became the worst due to oscillation. As can be seen the figure, both the mirror methods outperformed the LM-projected method in all the robots. In particular, the JT-mirror method clearly reduced the update amount while it kept the comparable tracking performance.

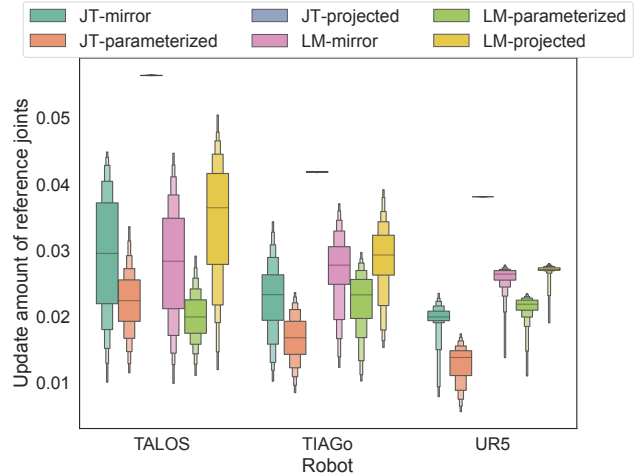


Fig. 6. Update amount of the reference joints at each time step in the tracking task: both the mirror methods improved smoothness of updates rather than the LM-projected method, while they have almost the comparable tracking performance; in particular, the JT-mirror method clearly reduced the update amount.

Examples of the above experiments can be seen in the following video uploaded on YouTube: <https://youtu.be/d03ZcdE0b5E>. In summary, it can be indicated that the JT-mirror method is the most useful in terms of low computational cost and stable performance, especially when running on machines with low computational power.

V. CONCLUSION

This paper proposed a new Jacobian-based IK solver explicitly considering box-constrained joint space. The problem in the clamping operation, which is the major approach in the conventional Jacobian-based IK to constrain the reference joints, has been pointed out that it causes numerical instability due to non-smoothed objective function. To alleviate the clamping problem, this study integrated the MD method, where the box-constrained real joint space is mapped to the no-constrained and invertible mirror space, with the conventional Jacobian-based IK methods, so-called MD-IK. In addition, to escape local optima nearly on the boundaries of constraints, ϵ -clamping is heuristically implemented as margin at software level. The numerical experiments statistically verified that MD-IK achieved more stable and enough fast i) regulation on the random reference poses and ii) tracking to the random trajectories compared to the conventional IK solvers. Remarkably, MD-IK with the JT gradient computation outperformed the LM-based gradient computation under most conditions.

In the future, by re-deriving IK as a constrained optimization problem, the gradient computation suitable for the MD method will be considered. As a practical application, we can investigate the whole-body motion (e.g. locomotion) performance when MD-IK is used for real humanoid robots.

APPENDIX

A. Derivation of MD-IK with logistic function

The term of σ in eq. (16) is derived as follows:

$$\begin{aligned}
 & \sigma(\sigma^{-1}(\mathbf{q}^{\text{nom}}) - \alpha \mathbf{g}(\mathbf{q}^{\text{ref}})) \\
 &= \frac{1}{1 + \exp\left(-a\left(-\frac{1}{a} \log \frac{1 - \mathbf{q}^{\text{nom}}}{\mathbf{q}^{\text{nom}}} + b - \alpha \mathbf{g}(\mathbf{q}^{\text{ref}}) - b\right)\right)} \\
 &= \frac{1}{1 + \exp\left(\log \frac{1 - \mathbf{q}^{\text{nom}}}{\mathbf{q}^{\text{nom}}} + a\alpha \mathbf{g}(\mathbf{q}^{\text{ref}})\right)} \\
 &= \frac{1}{1 + \frac{1 - \mathbf{q}^{\text{nom}}}{\mathbf{q}^{\text{nom}}} \exp(a\alpha \mathbf{g}(\mathbf{q}^{\text{ref}}))} \\
 &= \frac{\mathbf{q}^{\text{nom}}}{\mathbf{q}^{\text{nom}} + (1 - \mathbf{q}^{\text{nom}}) \exp(a\alpha \mathbf{g}(\mathbf{q}^{\text{ref}}))} \quad (23)
 \end{aligned}$$

By denormalizing the above, eq. (21) is obtained.

REFERENCES

- [1] M. Hirose and K. Ogawa, "Honda humanoid robots development," *Philosophical Transactions of the Royal Society A: Mathematical, Physical and Engineering Sciences*, vol. 365, no. 1850, pp. 11–19, 2007.
- [2] T. Asfour, L. Kaul, M. Wächter, S. Ottenhaus, P. Weiner, S. Rader, R. Grimm, Y. Zhou, M. Grotz, F. Paus, *et al.*, "Armar-6: A collaborative humanoid robot for industrial environments," in *IEEE-RAS International Conference on Humanoid Robots*. IEEE, 2018, pp. 447–454.
- [3] M. Gienger, M. Toussaint, and C. Goerick, "Task maps in humanoid robot manipulation," in *IEEE/RSJ International Conference on Intelligent Robots and Systems*. IEEE, 2008, pp. 2758–2764.
- [4] D. H. P. Nguyen, M. Hoffmann, A. Roncone, U. Pattacini, and G. Metta, "Compact real-time avoidance on a humanoid robot for human-robot interaction," in *ACM/IEEE International Conference on Human-Robot Interaction*, 2018, pp. 416–424.
- [5] S. R. Buss, "Introduction to inverse kinematics with jacobian transpose, pseudoinverse and damped least squares methods," *IEEE Journal of Robotics and Automation*, vol. 17, no. 1-19, p. 16, 2004.
- [6] A. Aristidou, J. Lasenby, Y. Chrysanthou, and A. Shamir, "Inverse kinematics techniques in computer graphics: A survey," vol. 37, no. 6, pp. 35–58, 2018.
- [7] T. Sugihara, "Solvability-unconcerned inverse kinematics by the levenberg-marquardt method," *IEEE Transactions on Robotics*, vol. 27, no. 5, pp. 984–991, 2011.
- [8] P. Beeson and B. Ames, "TRAC-IK: An open-source library for improved solving of generic inverse kinematics," in *IEEE-RAS International Conference on Humanoid Robots*. IEEE, 2015, pp. 928–935.
- [9] D. A. Drexler and I. Harmati, "Joint constrained differential inverse kinematics algorithm for serial manipulators," *Periodica Polytechnica Electrical Engineering and Computer Science*, vol. 56, no. 4, pp. 95–104, 2012.
- [10] A. Aristidou and J. Lasenby, "FABRIK: A fast, iterative solver for the inverse kinematics problem," *Graphical Models*, vol. 73, no. 5, pp. 243–260, 2011.
- [11] B. Kenwright, "Inverse kinematics–cyclic coordinate descent (CCD)," *Journal of Graphics Tools*, vol. 16, no. 4, pp. 177–217, 2012.
- [12] T. Kobayashi, E. Dean-Leon, J. R. Guadarrama-Olvera, F. Bergner, and G. Cheng, "Multi-contacts force-reactive walking control during physical human-humanoid interaction," in *IEEE-RAS International Conference on Humanoid Robots*. IEEE, 2019, pp. 33–39.
- [13] J. Nakanishi, S. Itadera, T. Aoyama, and Y. Hasegawa, "Towards the development of an intuitive teleoperation system for human support robot using a vr device," *Advanced Robotics*, vol. 34, no. 19, pp. 1239–1253, 2020.
- [14] P. H. Calamai and J. J. Moré, "Projected gradient methods for linearly constrained problems," *Mathematical programming*, vol. 39, no. 1, pp. 93–116, 1987.
- [15] A. Beck and M. Teboulle, "Mirror descent and nonlinear projected subgradient methods for convex optimization," *Operations Research Letters*, vol. 31, no. 3, pp. 167–175, 2003.
- [16] N. Srebro, K. Sridharan, and A. Tewari, "On the universality of online mirror descent," in *Advances in neural information processing systems*, 2011, pp. 2645–2653.
- [17] J. Carpentier, G. Saurel, G. Buondonno, J. Mirabel, F. Lamiroux, O. Stasse, and N. Mansard, "The pinocchio c++ library: A fast and flexible implementation of rigid body dynamics algorithms and their analytical derivatives," in *IEEE/SICE International Symposium on System Integration*. IEEE, 2019, pp. 614–619.
- [18] O. Stasse, T. Flayols, R. Budhiraja, K. Giraud-Esclasse, J. Carpentier, J. Mirabel, A. Del Prete, P. Souères, N. Mansard, F. Lamiroux, *et al.*, "Talos: A new humanoid research platform targeted for industrial applications," in *IEEE-RAS International Conference on Humanoid Robotics*. IEEE, 2017, pp. 689–695.
- [19] J. Pages, L. Marchionni, and F. Ferro, "Tiago: the modular robot that adapts to different research needs," in *International workshop on robot modularity, IROS*, 2016.
- [20] P. M. Kebria, S. Al-Wais, H. Abdi, and S. Nahavandi, "Kinematic and dynamic modelling of ur5 manipulator," in *IEEE international conference on systems, man, and cybernetics*. IEEE, 2016, pp. 004 229–004 234.